CHAPTER

Fast axonal transport in isolated axoplasm from the squid giant axon

16

Yuyu Song*,§, Minsu Kang*,¶, Gerardo Morfini*,¶, Scott T. Brady*,¶,1

*Marine Biological Laboratory, Woods Hole, MA, USA

§Yale School of Medicine, Department of Genetics and Howard Hughes Medical Institute, Boyer Center, New Haven, CT, USA

¶Department of Anatomy and Cell Biology, University of Illinois at Chicago, Chicago, IL, USA

1Corresponding author: E-mail: stbrady@uic.edu

CHAPTER OUTLINE

Abstract

The giant axon of the squid provides a unique cell biological model for analyzing the biochemistry and cell biology of the axon. These axons may exceed 500 μm in diameter and can be readily dissected. Once the surrounding small axons and connective tissue are removed, the axoplasm can be extruded as an intact cylinder of isolated cytoplasm. This isolated axoplasm is morphologically indistinguishable from the intact axon, but without permeability barriers. Fast axonal transport will continue for more than 4 h after extrusion and can be visualized in real time. By perfusing defined concentrations of proteins and/or reagents into the axoplasm, this preparation represents a powerful model for study of intracellular trafficking and its underlying molecular mechanisms.

Methods in Cell Biology, Volume 131, ISSN 0091-679X, http://dx.doi.org/10.1016/bs.mcb.2015.07.004

The Neuronal Cytoskeleton, Motor Proteins, and Organelle Trafficking in the Axon, First Edition, 2016, 331–348

INTRODUCTION

The number of studies based on live cell imaging has exploded in the last decade as new methodologies were developed for tagging proteins, and high-resolution fluorescence imaging systems became widely available. However, these approaches are not always the only choice for addressing questions associated with intracellular trafficking of cellular proteins and structures.

If the primary question under review is about the properties of the motors moving proteins, then video-enhanced contrast–differential interference contrast (VEC-DIC) microscopy, as introduced by Robert Allen and his colleagues (Allen, 1985; Allen & Allen, 1983; Allen, Allen, & Travis, 1981), remains a unique tool for real-time analysis of vesicle trafficking. VEC-DIC is particularly powerful when used in combination with isolated axoplasm from the squid giant axon (Brady, Lasek, & Allen, 1982, 1985), where limitations in spatial resolution due to diffraction at cell edges are minimized. Suitable squid (*Loligo pealeii*) are available routinely at the Marine Biological Laboratory in Woods Hole, MA, USA, from April to November (Figure 1). VEC-DIC allows visualization of intracellular organelles moving at rates of up to 2–4 μm/s, which requires acquisition at rates of 30 frames per second (fps) or more. Moreover, it avoids the addition of tags to proteins of

FIGURE 1

The squid, *L. pealeii*, which is abundant in the North Atlantic waters off of Cape Cod from April through November, has giant axons suitable for extrusion. These are readily available from the Marine Resources Center at the Marine Biological Laboratory in Woods Hole, MA, USA. Unfortunately, the squid varieties most suitable for isolated axoplasm preparations are not easily maintained in captivity for extended periods and generally rely on availability of fresh caught squid.

interest, which may potentially alter their processing and/or compartmentalization. This is particularly worrisome when such proteins are overexpressed, or whenever those proteins are subunits of larger protein complexes, as the stoichiometry of components is critical for appropriate assembly.

In this chapter, we will first briefly describe the equipment and processing needed for VEC-DIC and then describe the isolation and preparation of the axoplasm. The consideration of technology will serve to illuminate several challenges presented by the need to image trafficking of organelles in cells, particularly neurons. Similarly, our discussion of the axoplasm will provide some insight into why the axon represents a specialized case of intracellular trafficking.

1. MICROSCOPY AND IMAGING

The foundation of this method remains real-time (30 fps) VEC-DIC microscopy. Objects below the diffraction limit of resolution (roughly 170 nm for green light) can be detected in live imaging. Objects that are readily imaged under the proper conditions include small vesicles in the 50–100 nm range and individual microtubules. The basis of this approach is conceptually simple: structures smaller than the diffraction limit still interact with photons but project an image that is comparable to the diffraction limit. However, the intensity of this projected image drops off very rapidly as fewer photons are distributed over the same diffraction-limited area. These faint images cannot be readily detected in a standard video image due to the high background intensity. The situation is analogous to the reason why stars are not visible at noon on a sunny day. Scattered light from the sun creates a background much brighter than the stars. Eliminating the scattered light from the sun would reveal the much fainter points of light from the stars.

1.1 MICROSCOPE AND IMAGING HARDWARE

The method developed by Allen et al. (Allen, 1985; Allen & Allen, 1983; Allen et al., 1981) uses real-time video enhancement of contrast on a live image to permit visualization of subresolution structures in three stages: (*1*) The black level of the video image is set to minimize background light. (*2*) Optical noise due to inhomogeneity in the illumination and dust in the light path is visualized by focusing just outside of the specimen and digitally stored. The same stored image is subtracted from all subsequent frames of the live video, thus minimizing optical noise. (*3*) Using the algorithms available through the image processor, the contrast range of the image is expanded to take full advantage of the display capabilities. The result is a remarkable enhancement of our ability to detect and follow subresolution (for DIC) cellular structures (cytoskeletal and vesicular) in real time in living cells without molecular manipulations. This method does not change the resolution of the optics, as the Rayleigh diffraction limit still applies, but it provides a powerful

visualization of subcellular structure and cell dynamics, one that remains unique in its ability to reveal details of a living cell (Salmon & Tran, 2007).

There are two approaches to obtaining these images of subcellular structures above: (*1*) the original approach was to use dedicated image processing hardware to generate and analyze the image; and (*2*) software-based image processing using general-purpose computers for analysis. Each of these approaches has benefits and challenges, which will be considered in turn. The critical requirement for any image processing solution is that it must permit analysis on live video at a minimum of 30 fps. Ideally, image processing can be done in real time as well, including subtraction of a frame from memory to remove optical noise, adjustment of black level, and expansion of contrast range.

Finally, a means to measure the speed of organelle traffic is needed. We utilize a method in which an observer matches the speed of a cursor to moving particles interactively. Note, this is not a *particle tracking algorithm*, which is commonly featured in software such as ImageJ, Metamorph, Volocity and others, nor is it the kymograph option that is similarly widespread. Neither of these methods can be used to analyze the full range of organelle traffic due to resolution limits and the density of traffic. As will be discussed below, the organelles of interest are almost all subresolution (for DIC) particles that are too densely packed to resolve as individual particles and that, in addition, may not remain in the plane of focus for extended periods of time. As a result of these constraints, individual particles cannot be defined and followed by conventional tracking software.

Our standard setup for analysis of vesicle trafficking in axoplasm is based on a Zeiss Axiomat with a 100x, 1.3 n.a. objective, an optivar set at 2x and full DIC optics. The Axiomat is ideal because of its unusual mechanical stability and wide field of view. However, in principle, any microscope with suitable high-resolution DIC optics and a stable platform could be used.

Our standard camera is a Model C2400 CCD with a Hamamatsu Argus 20, and the video is directed to a Hamamatsu Photonics Microscopy C2117 video manipulator for image adjustment and generation of calibrated cursors and scale bars. Unfortunately, the Argus 20 and Video Manipulator are no longer manufactured and no contemporary equivalent exists. A standard, high-resolution CCD with adjustable dynamic range and the ability to acquire images at $\geq$30 fps would be suitable.

In principle, software-based methods should be able to replicate the capabilities of this hardware version above. However, no off-the-shelf solution is currently available. The heavy emphasis on fluorescence-based imaging in recent years has led to approaches optimized for post hoc analysis and processing. Some of the standard versions are not able to do real-time processing (Image-Pro Plus) or have limited capability (Metamorph and Volocity). Customization of commercial products or open source software such as ImageJ is the most likely solution at present. We are currently in the process of developing such a customized system and will make the script available after it has been validated.

1.2 MICROSCOPE PROCEDURES

1. Focus on the axoplasm, just slightly up from the coverslip, using the 100x 1.3 n.a. objective and DIC microscopy optics with de Senarmont compensator (λ/4 wave plate) inserted and verify optimal Köhler illumination (Allen, 1985; Inoue & Spring, 1997). Even illumination is critical for optimal visualization of subresolution objects. Also, the use of a fiber-optic scrambler to reduce illumination of hot spots is recommended. Typically, the analyzer is set for 110 to maximize the signal.
2. Set the optivar zoom to two and insert reticle scale into field for calibration of video manipulator. Once true magnification is established, switch to speed estimation option to superimpose calibrated cursors onto image.
3. Adjust the focus to just outside the axoplasm and save the image. This will allow removal of mottle associated with optical noise in the optical path unrelated to the specimen and eliminate hot spots due to uneven illumination. This saved image will be continuously subtracted from the live video.
4. Refocus inside the axoplasm while remaining close to the coverslip, and then expand the contrast to use the full dynamic range of the camera/monitor.

2. PREPARATION OF ISOLATED AXOPLASM

Isolated axoplasm is a unique preparation that models in vivo conditions with considerable fidelity, preserving many aspects of the intracellular environment while allowing free access to the intracellular compartment. Perfusions may be limited to very small volumes in the absence of permeability barriers (20–25 μL for a 5 μL axoplasm is typical). Moreover, the concentration of perfusates can be controlled with great precision. Normally, applying proteins and drugs intracellularly faces several challenges: (1) partitioning across a membrane, even with the limited set of reagents that are membrane-permeable, can be difficult to assess; (2) microinjection is the only option for larger molecules, but uniform concentrations and specific levels of the injected molecules are difficult to achieve and measure. In the case of isolated squid axoplasm, the plasma membrane barrier (axolemma) is removed, and rates of diffusion into and out of the axoplasm have been directly measured (Morris & Lasek, 1984).

2.1 BUFFERS

One factor often overlooked in studies on intracellular proteins is the composition of intracellular buffers, which often bear little resemblance to those commonly used in biochemical studies. Whereas low ionic strength buffers are commonly employed in enzymological studies, intracellular environments are relatively high ionic strength (>600 mM), much of which is provided by organic ions such as amino acids. In particular, the levels of chaotropic anions like Cl^- are much lower than organic anions like aspartate and glutamate (Song & Brady, 2013). Early studies on transport in

axoplasm led to the creation of a simplified buffer modeled on the actual composition of the intracellular environment in squid axons, at least with regard to small molecular weight components, *Buffer X* (Brady, Lasek, & Allen, 1983; Brady et al., 1985) (see Table 1 and Chapter Biochemical Analysis of Axon-Specific Phosphorylation Events Using Isolated Squid Axoplasms). This buffer was found to preserve axoplasmic structure, maintaining the axoplasm as an intact structure for hours, while allowing free exchange of soluble components in and out of the axoplasm. Buffer X can be diluted to half strength (Buffer X/2) without significantly altering the amount or velocity of organelles (Brady, Richards, & Leopold, 1993). This dilution is the current standard condition that we use as it causes a slight swelling of the axoplasm due to greater separation of the cytoskeletal elements like microtubules and neurofilaments (Brown & Lasek, 1993). This increases the number of individual microtubules visible on the periphery of the axoplasm and facilitates visualization of organelle traffic in the axoplasm interior.

Aliquots of stock reagents may be combined as indicated in the table and the pH checked before final dilution. The pH should be adjusted to 7.2 with KOH if needed. The stock can be brought to a final volume with 20 mM HEPES, pH 7.2 and filtered on 45-mm Millipore filter or equivalent. Store in suitable aliquots at −20 °C until ready for use. We use full strength Buffer X with no added ATP to rinse the axon prior to extrusion (see below). For perfusions, we routinely prepare aliquots without ATP, but bringing the stock to 20 mL rather than the 25 mL final volume (Table 1). This Buffer X/0.8 is stored at −20 °C as 0.4 mL aliquots. Immediately prior to use, an aliquot is thawed and ATP added from a concentrated stock of 100 mM ATP to the desired concentration and the aliquot brought to a final volume of 0.5 mL to produce *Buffer X plus ATP*. Normal levels of ATP are roughly 1−5 mM for axonal transport studies, but we use 0.5−1 mM ATP for biochemical studies involving kinases. The *Buffer X plus ATP* stock is typically made at 2x final concentration of ATP (2 mM or 5 mM) to allow use as Buffer X/2.

2.2 DISSECTION AND EXTRUSION

1. Obtain a healthy translucent squid (*L. pealeii* or comparable species) sized ≥30 cm in length (Figures 1 and 2).
2. Hold the squid by its mantle and decapitate the specimen above its eyes using utility scissors. Make sure the brain is detached from the mantle after decapitation. See Table 2 for list of materials needed.
3. Cut the mantle open along the midline on the posterior surface (fins facing down) and pin the distal portion of the mantle on each side with 18-gauge syringe needles to keep the mantle spread on the table, as shown in Figure 3.
4. Remove the viscera by grabbing them at the base with tissue forceps and pulling gently, cutting or teasing the connective tissues underneath as necessary to free the viscera from mantle using surgical scissors.
5. Remove the pen by pulling it steadily from the top of the mantle. Be careful not to pull too hard or fast to avoid damaging the giant axons.

Table 1 Buffer X

Chemical	MW	M (in Stock)	Grams per 25 mL Stock	mM in Buffer X/2	mL Stock in 25 mL Buffer X
Potassium aspartate	171.2	1	4.28	175	8.75
Taurine	125.1	add by weight	add by weight	65	0.407 g
Betaine	135.2	1	3.38	35	1.75
Glycine	75.07	1	1.88	25	1.25
$MgCl_2 \cdot 6H_2O$	203.31	1	5.08	6.46	0.323
$K_2 \cdot$EGTA (adjust stock to pH 7.2 with KOH before bringing to final volume)	380.4	0.1	0.951	5	2.5
HEPES (adjust stock to pH 7.2 with KOH before bringing to final volume)	238.3	1	5.96	10	0.5
$CaCl_2 \cdot 2H_2O$	147.02	1	3.68	1.5	0.075
Glucose	180.2	0.1	0.4505	0.5	0.25
$K_2 \cdot$ATP (adjust stock to pH 7.2 with KOH before bringing to final volume)	583.4	0.2	2.92 (0.1167/mL)	1	0.25 mL stock, or 0.0292 g dry powder

The Neuronal Cytoskeleton, Motor Proteins, and Organelle Trafficking in the Axon, First Edition, 2016, 331–348

Table 2 Materials

Dissection table equipped with glass port and running seawater, and indirect, transmitted light source placed underneath (see Figure 3)
Low-power stereo dissection microscope on spring loaded tilting arm stand
Stereo dissection microscope with dark-field illumination
Filtered seawater (0.45 μm pore filtered), kept chilled in ice
Utility scissors (5″ or larger)
Trident II spring scissors (FST #15110-08) or Noyes spring scissors (14 mm edge)
Vannas spring scissors (straight, 4 mm edge)
Surgical scissors (sharp-blunt tips, 40–50 mm edge)
Dumont #5 (standard tip) and #5/45 forceps (biology tip), Titanium or Dumostar for resistance to corrosion in seawater
Tissue forceps 2x3 teeth (straight 14–15 cm)
Syringe needles (18-gauge)
Petri dish (P100)
Dental wax (Surgident Periphery Wax, Columbus Dental, St. Louis, MO)
2 x Petri dish with cover (P150)
Cotton threads in two different colors (e.g., black and white)
Buffer X for rinsing of freshly dissected axons before extrusion
0 thickness coverslips (24 × 60 mm)
0 thickness coverslips (22 × 22 mm)
Diamond tip pen for scoring glass to create spacers from the 0 thickness coverslips
Polyethylene tubing PE190, cut to ~4 cm length
VALAP (1:1:1 mix of Vaseline:Lanolin:Paraffin) kept melted on a heat block at 50 °C

6. Flip the mantle so that the skin and fins are facing up and secure the mantle with the 18-gauge syringe needles.
7. Remove the fins with surgical scissors, and peel the skin off by grasping with tissue forceps and pulling apart from underlying muscle. Removing the pigmented skin leaves a translucent mantle.
8. Flip the mantle so that the posterior surface is facing up. The pair of giant axons lying parallel to the midline on each side should be visible (Figures 2 and 3).
9. For the rough dissection of the axon, grasp the tissue surrounding the giant axon with Dumont forceps and carefully free up a 2–3 cm portion of a giant axon by separating the axon bundle from the mantle using forceps, and Trident or Noyes spring scissors. Start near the stellate ganglion and progress distally, leaving connective tissue/smaller axon bundles attached. Avoid touching the giant axon itself during the dissection as it may damage the axolemma, creating leaks. The giant axon is intact at this point with its sheath and associated smaller axons/connective tissue still attached (Figure 3).
10. Repeat Step 9 with the other giant axon.

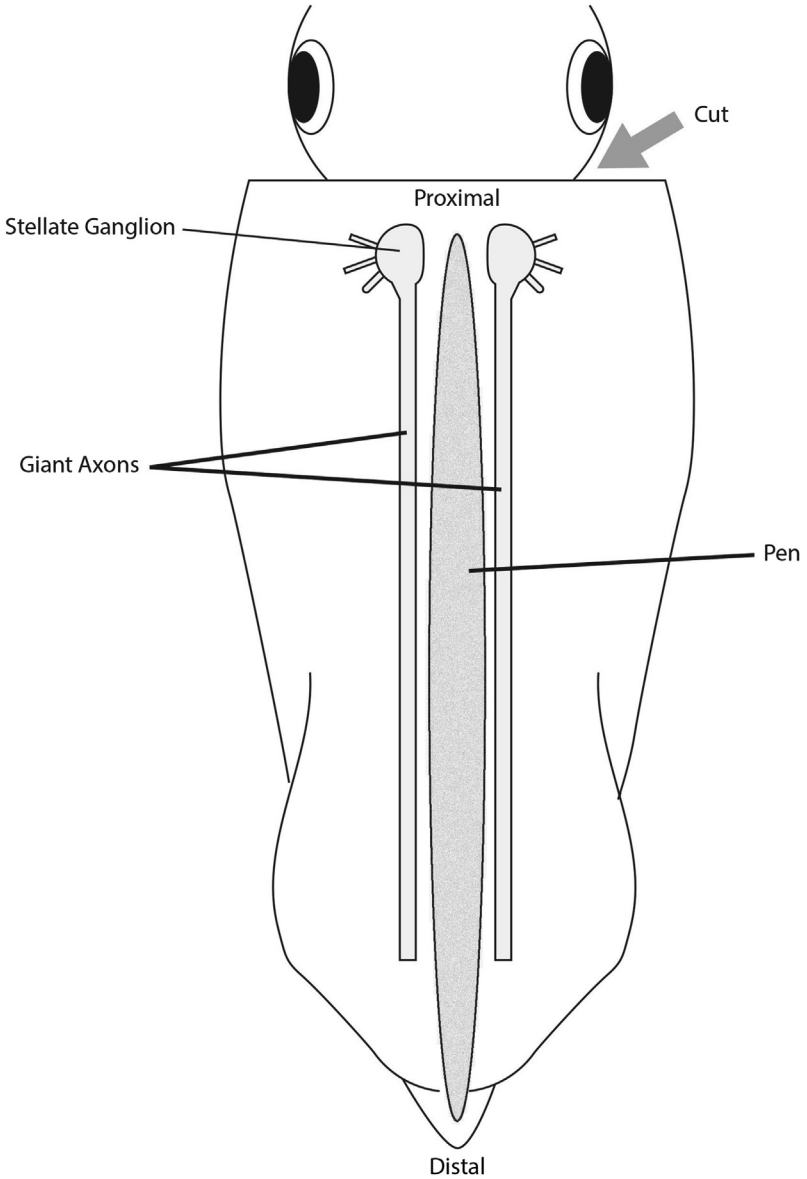

FIGURE 2

Schematic diagram for position of stellate ganglion and giant axons used in isolated axoplasm preparations. Although each stellate axon gives rise to multiple giant axons, only the largest and longest ones paralleling the midline of the squid can be used reliably. Axons must be >250 μm in diameter to extrude properly and axons 400–500 μm in diameter are preferred.

FIGURE 3

Squid mantle on dissecting table with transillumination and running seawater. This illustrates our standard configuration for the rough dissection of the two giant axons used from each squid.

11. Using a white cotton thread (cut ~10 cm), tie off the proximal end of the giant axon near the stellate ganglion and trim one end of the thread with surgical scissors.
12. Using a black cotton thread (cut ~10 cm), tie the distal end of the giant axon making sure that you have 2.5–3 cm of axon, then trim one end of the thread. The two colors help assure that orientation of the axon is preserved.
13. Repeat Step 11 and Step 12 with the other "sister" axon (see Chapter Biochemical Analysis of Axon-Specific Phosphorylation Events Using Isolated Squid Axoplasms).
14. Fix dental wax in place on the edges of the P100 Petri dish to hold the pins for securing the threads, then place the P100 in the center of P150 dish and pack the remaining area of P150 loosely with ice (Figure 4).
15. Fill the P100 Petri dish with ice-cold filtered seawater and place two 18-gauge needle tips on opposite sides of the Petri dish about 5 cm apart from each other (Figure 4(A)).
16. Cut the giant axons 5 mm away from the knots to detach the giant axons using Trident or Noyes spring scissors.
17. Suspend the axons in ice-cold filtered seawater by wrapping the thread around the needle tips and place them under a stereo dissection microscope with dark-field illumination for fine dissection.
18. Gently tease away small axons and connective tissue using Vannas-style iris scissors and No. 5 Dumont forceps. The axon appears clear under dark-field

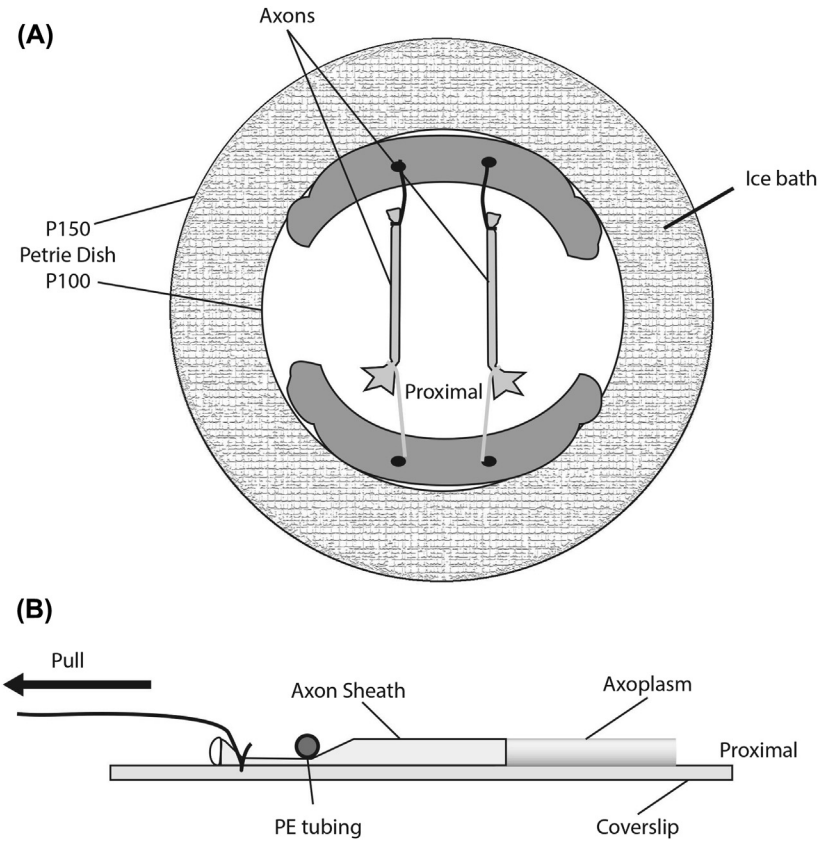

FIGURE 4

Fine dissection and extrusion of axoplasm. (A) Once the giant axons are removed from the squid, they are positioned in a Petri dish (P100), secured by threads using 18-gauge syringe needles and dental wax for fine dissection and cleaning of giant axon. The Petri dish is filled with cold, filtered seawater and placed in a larger Petri dish (P150) in an ice bath. (B) After removal of connective tissue and small axons, the giant axon is transferred from the seawater bath, rinsed in Buffer X, blotted on filter paper and placed on a coverslip. Held by the black (distal) thread, the axon is cut near the proximal (white) thread. This orientation is preferred for extrusion as the distal axon may be slightly smaller in diameter due to the occurrence of branches. To extrude the axoplasm, a piece of PE190 tubing is used to apply pressure to the distal axon and the axon is drawn through the constriction by being pulled on the distal thread.

illumination, while the connective tissue surrounding the axon appears white or gray. The connective tissue is threadlike, which can be carefully teased away from the axon using No. 5 Dumont forceps and trimmed as necessary using Vannas iris scissors. Use care to avoid excess tension on the giant axon, which can easily break during fine dissection. Do not put the blades of the

scissors directly on the axon and avoid tearing small branches that should be cut a millimeter or so from the surface of the giant axon.

19. When the fine dissection is complete, the giant axon appears as a clear tube with a clean surface. Inspect for cloudy or white patches in the axon, which are a sign that the axolemma has been damaged and seawater containing Ca^{2+} has entered the axon, causing local proteolysis. Damaged axons should be discarded.
20. Repeat Step 18 with the other giant axon.
21. Detach the fine-dissected axons from the needle tips by carefully unwrapping the thread that secured the axons, avoiding pulling of the axon.
22. Briefly blot the axons on a piece of No. 2 filter paper.
23. Rinse the axons in Buffer X and blot to remove excess Buffer X on No. 2 filter paper.
24. Rinse the Vannas-style iris scissors and No. 5 Dumont forceps in Buffer X and blot them on the filter paper.
25. Place one axon on a 24 × 60 coverslip secured on a slide holder with tape. For biochemical studies, the extrusion can be done on a clean, standard glass microscope slide (see Chapter Biochemical Analysis of Axon-Specific Phosphorylation Events Using Isolated Squid Axoplasms).
26. Cut the proximal end of the axon just distal of the white thread, check to see that a small amount of axoplasm oozes out.
27. Hold the axon by the black thread and press the polyethylene tubing near the distal end. Steadily pull the axon by the black thread, keeping the tubing stationary, to extrude the axoplasm. This should leave a cylinder of axoplasm on the microscope slide with intact organization and structural integrity (Figure 4(B)).
28. Carefully coat previously prepared spacers (≈3 × 22 mm 0 thickness glass) with a thin layer of Molykote Compound 111 (Dow Corning) silicone lubricant. Do not use vacuum grease, which will leach into the perfusate. Place one spacer on either side of the extruded axoplasm, taking care not to smear the silicone lubricant or touch the axoplasm. Carefully place a 22 × 22 mm 0 thickness coverslip on top without shearing the axoplasm. This will create a coverslip sandwich in which the axoplasm contacts both coverslip surfaces (Figure 5(A)).
29. Secure the top coverslip in place and seal the area of the spacers by placing a drop of melted VALAP with a wooden swab. Leave the ends open to allow perfusion (see Figure 5(B)).
30. Preincubate the slide chamber with the axoplasm for 15 min in a humidified chamber kept at 4 °C prior to use. This improves reproducibility of the axoplasms. After the 15 min of preincubation, the axoplasms can be kept in a humidified chamber for 2−3 h at room temperature prior to analysis.
31. Repeat Steps 24−30 with the other "sister" axon.

2.3 PERFUSION

Axoplasms may be perfused with Buffer X/2 + 1−5 mM ATP containing experimental agents of interest, including disease-related proteins (wild-type and

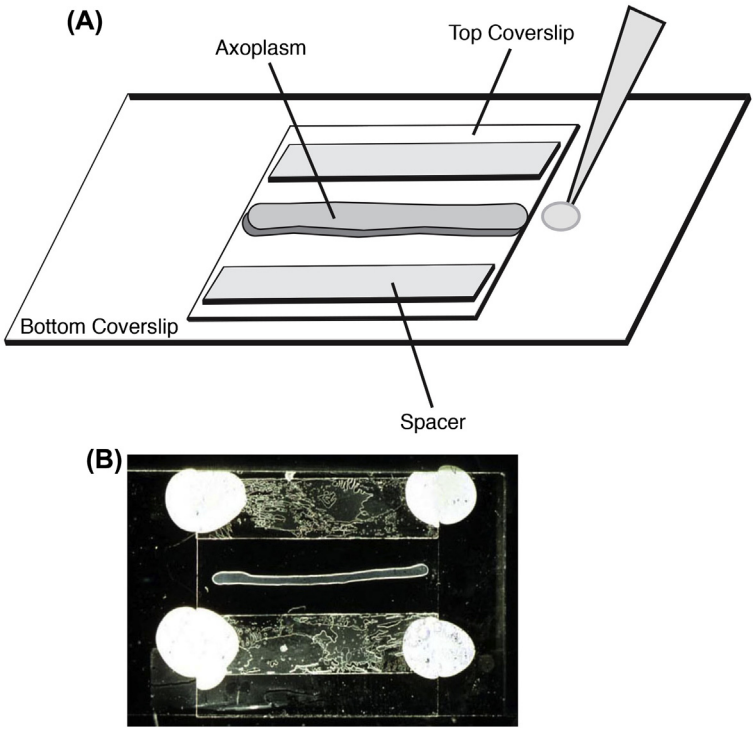

FIGURE 5

Perfusion and imaging chamber. (A) Diagram of axoplasm chamber and position of pipette tip for adding perfusion. The axoplasm is extruded onto a 24 × 60 mm 0 thickness coverslip, then two spacers are placed on either side of the axoplasm secured with Molykote 111. A small (22×22) square 0 thickness coverslip is placed on top so the axoplasm makes contact with both top and bottom coverslips. Care must be taken not to shear the axoplasm. The chamber has a volume of 20–25 μL with space on both sides of the axoplasm and open ends to allow perfusion. (B) Assembled chamber with top coverslip secured by VALAP.

pathogenic), enzymes, antibodies, peptides, or pharmacological agents (see Chapter Biochemical Analysis of Axon-Specific Phosphorylation Events Using Isolated Squid Axoplasms). Typically, proteins of interest with or without pharmacological agents are added at twice the desired final concentration in 50 mM HEPES, pH 7.2 (see Chapter Biochemical Analysis of Axon-Specific Phosphorylation Events Using Isolated Squid Axoplasms for examples). For imaging experiments, aliquots of the protein effector with or without inhibitors are diluted in 50 mM HEPES, pH 7.2, and added to an equal volume of *Buffer X plus ATP*, such that the final perfusate mixture consists of Buffer X/2 plus ATP plus the effectors of interest. Perfusate volumes are kept small relative to the axoplasm volume (roughly 5 μL) to minimize dilution. The standard volume of a perfusion is 20–25 μL, leading to a dilution factor of 3–4. In contrast, conventional biochemical approaches will often involve

dilutions of cell constituents by a factor or 10^3−10^5 times or even more (Song & Brady, 2013), dramatically affecting low affinity protein−protein interactions.

Before perfusion, the axoplasm is placed on the microscope stage and imaged as described in Section 1. Preperfusion transport rates are measured for each axoplasm to assure that anterograde rates are within 1.5−2 μm/s range and retrograde rates are within 1.1−1.5 μm/s range. If squids have been stressed due to elevated water temperature or excessive handling, preperfusion rates may be lower, in which case the axoplasm is discarded.

Healthy axoplasms are perfused on the microscope stage using a PR200 or PR100 manual pipette (Rainin). The tip of the pipette containing the perfusate is placed carefully near the opening of the axoplasm chamber (Song & Brady, 2013). We routinely perfuse from the proximal end, although this is not critical. Transverse illumination with a small lantern is helpful in visualizing the edge of the chamber. Care must be taken to avoid pressing on the coverslip. Slowly add the perfusate so it makes contact with the chamber's edge (Figure 5(A)). Capillary action will rapidly draw the perfusate into the chamber and a timer is started. A good perfusion will roughly fill the chamber with perfusate on both sides of the axoplasm. This can be verified on the microscope by moving to the edge of the axoplasm and determining that the air/axoplasm boundary has been eliminated.

2.4 MEASUREMENT OF AXONAL TRANSPORT

The challenge of measuring total vesicle transport stems from a combination of limits to optical resolution and the sheer number of organelles moving in a given field. With the exception of mitochondria, most organelles in transport range in size from 50 to 150 nm in diameter, and microtubules are only 25 nm in diameter, all of which are well below the resolution limit for DIC microscopy. This limit is due to diffraction and is roughly 200 nm in the X-Y plane for polarized, monochromatic green light ($\lambda = 510$ nm) using matched, fully corrected, high numerical aperture (>1.3 n.a.) objectives and condensers. VEC-DIC can detect objects as small as individual microtubules that are well separated from other structures. However, when the objects are less than 200 nm apart, individual structures cannot be resolved from each other.

The situation above is further complicated because the axoplasm is a three-dimensional structure. The vertical resolution is approximately twice the horizontal resolution, so we are viewing particles present within a 400 nm optical section. Of course, the organelles and microtubules are not confined to this optical section and may enter and leave the optical section many times during transit of a 25 μm field of view. As a result, individual organelles other than mitochondria typically cannot be identified and followed by software-based tracking algorithms. Even larger organelles like mitochondria and large endosomes may appear and disappear from the field of view.

Despite this limitation, the flow of organelle traffic is easily detected by eye, and the apparent speed rate of that flow can be determined interactively during live

imaging or on recorded videos. The procedure routinely employed in our laboratory uses calibrated cursors generated by the Hamamatsu C2117 video manipulator that sweep across the field with a user-determined direction and rate. The observers match the speed and direction of the cursor movement interactively, and the rates recorded are only visible after the speed of the cursors matches that of the flowing vesicles. Normally, multiple observers are involved and the matching of cursor speed is reached by consensus. By alternately measuring anterograde and retrograde transport rates at regular intervals for 50 min, the effect of a given perfusate on fast axonal transport can be evaluated.

In a healthy axoplasm perfused with Buffer X/2 plus ATP without effectors, the speed rates obtained with the methods above are comparable to the rates obtained by tracking individual organelles on isolated microtubules at the periphery of the axoplasm. However, the effect of optical sectioning means that the rates obtained by this method in the interior of the axoplasm are a function of *both* the rate of movement along a microtubule and the frequency at which individual organelles enter and leave the 400 nm optical section, which in turn depends on the density of organelle trafficking at any given time. Treatments that slow the average rate of an organelle moving along a microtubule will produce a reduced rate both in the interior of the axoplasm and on individual microtubules. Such effect has been observed after perfusion of nucleotides that affect the ATPase activity of molecular motors (Leopold, Snyder, Bloom, & Brady, 1990). In contrast, other treatments may not affect the average rate of an organelle moving along single microtubules, yet measurements in the interior of the axoplasm yield slower rates. In such cases, this apparent reduction in rates results from reduced frequency of organelles entering and exiting the 400 nm optical section, which gives the appearance of a slower movement for the organelles. Such an effect has been observed after perfusion of kinases that promote detachment of conventional kinesin from transported organelles (i.e., GSK-3 (Morfini et al., 2004; Morfini, Szebenyi, Elluru, Ratner, & Brady, 2002)) or from kinases that compromise the binding of conventional kinesin to axonal microtubules (i.e., JNK3 (Morfini et al., 2009)).

SUMMARY

Although the isolated axoplasm model is not widely available, it has a number of unique characteristics that make it an invaluable model for studying cell biology and molecular biochemistry of the axon (see Chapter Biochemical Analysis of Axon-Specific Phosphorylation Events Using Isolated Squid Axoplasms). The squid giant axon is the only reliable source of pure axoplasm in its native state, allowing unparalleled access to a pure cytoplasmic fraction that is undiluted and retains its organization. Although the phylogeny of the squid suggests that it diverged from the vertebrate line about the same time as Drosophila, the cell biology has been preserved with remarkable fidelity regarding motor proteins, cytoskeletal elements, and signaling pathways. Not only did the squid axoplasm preparation provide the first

evidence for the kinesin family of motor proteins (Brady, 1985; Lasek & Brady, 1985; Vale, Reese, & Sheetz, 1985) and generate insights on the dynamics of the axonal cytoskeleton (Morris & Lasek, 1982, 1984; Pant, Shecket, Gainer, & Lasek, 1978; Song & Brady, 2013), but it also has identified a variety of signaling pathways that regulate organelle trafficking (Bloom, Richards, Leopold, Ritchey, & Brady, 1993; Morfini et al., 2004; Morfini et al., 2002; Ratner, Bloom, & Brady, 1998). Remarkably, the axoplasm has also proven to be a powerful model to probe the molecular basis of pathogenic proteins ranging from Alzheimer's disease (Kanaan et al., 2011; Lapointe et al., 2009; Pigino et al., 2009), Huntington's disease and other polyglutamine expansion diseases (Morfini et al., 2006; Morfini et al., 2009; Szebenyi et al., 2003), and amyotrophic lateral sclerosis (Bosco et al., 2010; Morfini et al., 2013; Song et al., 2013), among others. These experiments took advantage of squid as a unique model system and VEC-DIC as a matchless imaging tool to elucidate molecular pathways underlying axonal transport, which is extremely difficult to achieve in other systems. More importantly, these results have been consistently validated in mammalian animal models and human nerve tissue, thus demonstrating the relevance of the isolated axoplasm model for the study of physiological and pathological conditions in the human nervous system.

ACKNOWLEDGMENTS

The authors would like to express their gratitude to the many students who have spent summers at the Marine Biological Laboratory measuring fast axonal transport in axoplasm for their invaluable work at the MBL. Many of these students have been come from Hunter College, NY, through the HHMI summer research program. This work was mainly supported by grants from the National Institute of Health [NS066942A (to GM), and NS23868, NS23320, NS41170 (to STB)] and from HHMI and the Grass Foundation (YS).

REFERENCES

Allen, R. D. (1985). New observations on cell architecture and dynamics by video-enhanced contrast optical microscopy. *Annual Review of Biophysics and Biophysical Chemistry, 14*, 265–290. http://dx.doi.org/10.1146/annurev.bb.14.060185.001405.

Allen, R. D., & Allen, N. S. (1983). Video enhanced microscopy with a computer frame memory. *Journal of the Microscopy, 129*, 3–17.

Allen, R. D., Allen, N. S., & Travis, J. L. (1981). Video-enhanced contrast, differential interference contrast (AVEC-DIC) microscopy: a new method capable of analyzing microtubule related movement in the reticulopodial network of Allogromia laticollaris. *Cell Motility, 1*, 291–302.

Bloom, G. S., Richards, B. W., Leopold, P. L., Ritchey, D. M., & Brady, S. T. (1993). GTPγS inhibits organelle transport along axonal microtubules. *Journal of Cell Biology, 120*, 467–476.

Bosco, D. A., Morfini, G., Karabacak, N. M., Song, Y., Gros-Louis, F., Pasinelli, P., et al. (2010). Wild-type and mutant SOD1 share an aberrant conformation and a common pathogenic pathway in ALS. *Nature Neuroscience, 13*(11), 1396–1403. http://dx.doi.org/10.1038/nn.2660. pii:nn.2660.

Brady, S. T. (1985). A novel brain ATPase with properties expected for the fast axonal transport motor. *Nature, 317*, 73–75.

Brady, S. T., Lasek, R. J., & Allen, R. D. (1982). Fast axonal transport in extruded axoplasm from squid giant axon. *Science, 218*, 1129–1131.

Brady, S. T., Lasek, R. J., & Allen, R. D. (1983). Fast axonal transport in extruded axoplasm from squid giant axon. *Cell Motility, 3* (Video Supplement).

Brady, S. T., Lasek, R. J., & Allen, R. D. (1985). Video microscopy of fast axonal transport in isolated axoplasm: a new model for study of molecular mechanisms. *Cell Motility, 5*, 81–101.

Brady, S. T., Richards, B. W., & Leopold, P. L. (1993). Assay of vesicle motility in squid axoplasm. *Methods in Cell Biology, 39*, 191–202.

Brown, A., & Lasek, R. J. (1993). Neurofilaments move apart freely when released from the circumferential constraint of the axonal plasma membrane. *Cell Motility and the Cytoskeleton, 26*(4), 313–324.

Inoue, S., & Spring, K. R. (1997). *Video microscopy. The fundamentals* (2nd ed.). New York: Plenum Press.

Kanaan, N. M., Morfini, G. A., Lapointe, N. E., Pigino, G. F., Patterson, K. R., Song, Y., et al. (2011). Pathogenic forms of tau inhibit kinesin-dependent axonal transport through a mechanism involving activation of axonal phosphotransferases. *The Journal of Neuroscience: Official Journal of Society for Neuroscience, 31*(27), 9858–9868. http://dx.doi.org/10.1523/JNEUROSCI.0560-11.2011.

Lapointe, N. E., Morfini, G., Pigino, G., Gaisina, I. N., Kozikowski, A. P., Binder, L. I., et al. (2009). The amino terminus of tau inhibits kinesin-dependent axonal transport: Implications for filament toxicity. *Journal of Neuroscience Research, 87*(2), 440–451.

Lasek, R. J., & Brady, S. T. (1985). Attachment of transported vesicles to microtubules in axoplasm is facilitated by AMP-PNP. *Nature, 316*, 645–647.

Leopold, P. L., Snyder, R., Bloom, G. S., & Brady, S. T. (1990). Nucleotide specificity for the bidirectional transport of membrane-bounded organelles in isolated axoplasm. *Cell Motility and the Cytoskeleton, 15*, 210–219.

Morfini, G., Pigino, G., Szebenyi, G., You, Y., Pollema, S., & Brady, S. T. (2006). JNK mediates pathogenic effects of polyglutamine-expanded androgen receptor on fast axonal transport. *Nature Neuroscience, 9*, 907–916.

Morfini, G., Szebenyi, G., Brown, H., Pant, H. C., Pigino, G., DeBoer, S., et al. (2004). A novel CDK5-dependent pathway for regulating GSK3 activity and kinesin-driven motility in neurons. *EMBO Journal, 23*, 2235–2245.

Morfini, G., Szebenyi, G., Elluru, R., Ratner, N., & Brady, S. T. (2002). Glycogen synthase kinase 3 phosphorylates kinesin light chains and negatively regulates kinesin-based motility. *EMBO Journal, 23*, 281–293.

Morfini, G. A., Bosco, D. A., Brown, H., Gatto, R., Kaminska, A., Song, Y., et al. (2013). Inhibition of fast axonal transport by pathogenic SOD1 involves activation of p38 MAP kinase. *PLoS One, 8*(6), e65235. http://dx.doi.org/10.1371/journal.pone.0065235.

Morfini, G. A., You, Y. M., Pollema, S. L., Kaminska, A., Liu, K., Yoshioka, K., et al. (2009). Pathogenic huntingtin inhibits fast axonal transport by activating JNK3 and

phosphorylating kinesin. *Nature Neuroscience, 12*(7), 864–871. http://dx.doi.org/10.1038/nn.2346. pii:nn.2346.

Morris, J., & Lasek, R. J. (1982). Stable polymers of the axonal cytoskeleton: the axoplasmic ghost. *Journal of Cell Biology, 92*, 192–198.

Morris, J., & Lasek, R. J. (1984). Monomer-polymer equilibria in the axon: direct measurement of tubulin and actin as polymer and monomer in axoplasm. *Journal of Cell Biology, 98*, 2064–2076.

Pant, H. C., Shecket, G., Gainer, H., & Lasek, R. J. (1978). Neurofilament protein is phosphorylated in the squid giant axon. *Journal of Cell Biology, 78*(2), R23–R27.

Pigino, G., Morfini, G., Atagi, Y., Deshpande, A., Yu, C., Jungbauer, L., et al. (2009). Disruption of fast axonal transport is a pathogenic mechanism for intraneuronal amyloid beta. *Proceedings of the National Academy of Sciences of the United States of America, 106*(14), 5907–5912. http://dx.doi.org/10.1073/pnas.0901229106.

Ratner, N., Bloom, G. S., & Brady, S. T. (1998). A role for Cdk5 kinase in fast anterograde axonal transport: novel effects of olomoucine and the APC tumor suppressor protein. *Journal of Neuroscience, 18*, 7717–7726.

Salmon, E. D., & Tran, P. (2007). High-resolution video-enhanced differential interference contrast light microscopy. *Methods in Cell Biology, 81*, 335–364. http://dx.doi.org/10.1016/S0091-679X(06)81016-2.

Song, Y., & Brady, S. T. (2013). Analysis of microtubules in isolated axoplasm from the squid giant axon. *Methods in Cell Biology, 115*, 125–137. http://dx.doi.org/10.1016/B978-0-12-407757-7.00009-8.

Song, Y., Nagy, M., Ni, W., Tyagi, N. K., Fenton, W. A., Lopez-Giraldez, F., et al. (2013). Molecular chaperone Hsp110 rescues a vesicle transport defect produced by an ALS-associated mutant SOD1 protein in squid axoplasm. *Proceedings of the National Academy of Sciences of the United States of America, 110*(14), 5428–5433. http://dx.doi.org/10.1073/pnas.1303279110.

Szebenyi, G., Morfini, G. A., Babcock, A., Gould, M., Selkoe, K., Stenoien, D. L., et al. (2003). Neuropathogenic forms of huntingtin and androgen receptor inhibit fast axonal transport. *Neuron, 40*, 41–52.

Vale, R. D., Reese, T. S., & Sheetz, M. P. (1985). Identification of a novel force-generating protein, kinesin, involved in microtubule-based motility. *Cell, 42*, 39–50.